

LA-UR- 97-2074

Title: Growth-Related Magnetic and Physical Structures In CMS Films

CONF-970568--

Author(s):

Marilyn E. Hawley, CMS
Geoffrey W. Brown, CMS
Michael F. Hundley, MST-10
J.D. Thompson, MST-10
D.K. Hristova, MST-10
J. Tesmer, MST-10
Q.X. Jia, STC
E.J. Peterson, STC

RECEIVED

AUG 27 1997

O.S.T.I

Submitted to:

American Ceramic Society's 99th Annual Meeting.
Transactions of the American Ceramics Society May4-7, 1997
Cincinnati, OH
99th Annual Symposium

MASTER

Los Alamos

NATIONAL LABORATORY

Los Alamos National Laboratory, an affirmative action/equal opportunity employer, is operated by the University of California for the U.S. Department of Energy under contract W-7405-ENG-36. By acceptance of this article, the publisher recognizes that the U.S. Government retains a nonexclusive, royalty-free license to publish or reproduce the published form of this contribution, or to allow others to do so, for U.S. Government purposes. The Los Alamos National Laboratory requests that the publisher identify this article as work performed under the auspices of the U.S. Department of Energy.

DISTRIBUTION OF THIS DOCUMENT IS UNLIMITED

Form No. 836 R5
ST 2629 10/91

hf

DISCLAIMER

This report was prepared as an account of work sponsored by an agency of the United States Government. Neither the United States Government nor any agency thereof, nor any of their employees, make any warranty, express or implied, or assumes any legal liability or responsibility for the accuracy, completeness, or usefulness of any information, apparatus, product, or process disclosed, or represents that its use would not infringe privately owned rights. Reference herein to any specific commercial product, process, or service by trade name, trademark, manufacturer, or otherwise does not necessarily constitute or imply its endorsement, recommendation, or favoring by the United States Government or any agency thereof. The views and opinions of authors expressed herein do not necessarily state or reflect those of the United States Government or any agency thereof.

DISCLAIMER

Portions of this document may be illegible in electronic image products. Images are produced from the best available original document.

GROWTH-RELATED MAGNETIC AND PHYSICAL STRUCTURES IN CMR FILMS

M.E. Hawley

G.W. Brown

Center for Materials Science, MS K765

M.F. Hundley

J.D. Thompson

D.K. Hristova

J. Tesmer

Materials Science and Technology Division (MST-10), MS K764

Q.X. Jia

E.J. Peterson

Superconductivity Technology Center, MS K763

Los Alamos National Laboratory

Los Alamos, NM 87545

ABSTRACT

Scanning tunneling microscopy (STM), atomic force microscopy (AFM), and magnetic force microscopy (MFM) have proven to be powerful tools for revealing property-sensitive structures in magnetic materials. With the renewed interest in perovskite films as materials for read-heads in high-density magnetic data storage, the same challenges faced by high temperature superconductor (HTS) film fabrication are repeated for these materials. To begin addressing these challenges, we used vapor phase epitaxy to fabricate La (Sr, Ca,) based manganate films on single crystal perovskite substrates under different conditions and characterized them with scanning probe microscopies, x-ray diffraction, and temperature-dependent magnetization and resistivity measurements ($M(T)$ and $\rho(T)$). The as-grown films were polygranular with grain sizes increasing with increasing temperature (T). The post-deposition annealed films consisted of coalesced layers with improved transport properties. The room temperature magnetic structure of the Sr-based films appeared to be related to defects and/or strain.

INTRODUCTION

Over the last few years, there has been renewed activity in studying one group of materials within the rich perovskite family, ABO_3 . The perovskite structure is shown in Figure 1 with dopant substitutions on the La sites. The hole-doped

LaMnO₃ analogs, La_{1-x}M_xMnO₃ with M = Ca, Sr, or Ba (LCMO, LSMO, or LBMO), have been the center of most of this activity for potential use in a number of applications which can generally be classified as sensors. This potential relies on the large magnetoresistance (MR) effect exhibited by these materials. The MR is written as

$$MR \equiv \frac{\rho(H) - \rho(H=0)}{\rho(H=0)} \quad (1)$$

where $\rho(H)$ is the magnetic-field-dependent resistivity [1,2]. The peak MR occurs at the ferromagnetic ordering temperature, T_c , which coincides with the metal-insulator transition. Because $\rho(H) - \rho(H=0)$ is so large, the expression "colossal" magnetoresistance (CMR) has been associated with these materials. Empirically, it is found that, at any given temperature, the resistivity varies exponentially with the magnetization, implying that the transport is controlled by the magnetization that develops near and below T_c [1].

The sensitivity of the transport and magnetic properties to both the dopant level and the oxygen content make it possible to chemically engineer the material to suit a particular application, but this also presents materials synthesis and characterization problems. Additionally, for most of these applications, these materials will be used singly in thin film form or in a multilayer structure, adding vapor phase synthesis complications to these challenges. Most of our recent work has, therefore, been focused on understanding the role of deposition parameters in generating the resultant microstructure, defects, and properties. Drawing on the wealth of experience gained from the fabrication of high quality HTS films of YBa₂Cu₃O_{7-x} [3] our group [4,5], like many others [6-8] now involved in studying other perovskite films, has been able to produce high quality versions of the magnetic oxides.

Progress has been made in understanding the properties of bulk CMR material [9-11] but for films, attempts at systematically correlating particular growth parameters with changes in properties has, while showing trends, resulted in too many unanswered questions. For example, although it is well known that varying the growth temperature leads to changes in the physical microstructure, (i.e. grain size and orientation, lattice-mismatch and defect-induced strain), it is unclear whether the stoichiometry, particularly the oxygen content, remains constant. In addition, it is not obvious whether changes in T-dependent transport are linked to film structure or chemical variations. Most likely it is a combination of both. For the broad class of oxide films, whether the films are grown by pulsed-laser (PLD),

magnetron sputtering, or chemical vapor deposition methods, most fabrication parameters are inter-related. For example, the chamber pressure cannot be changed without also changing the plasma shape, size, or species energetics, which in turn directly impacts of the growth kinetics. The roles of lattice-mismatch and deposition parameters in the generation of stress and defect structures in the growing film are also not fully understood.

In the present work we have focused primarily on the growth of LSMO films and have limited the variables to two parameters: 1) the *substrate material* and 2) the *substrate temperature*, T_S . We used single crystal LaAlO_3 (LAO) and SrTiO_3 (STO) substrates and grew films at $T_S = 500^\circ\text{C}$, 650°C , and 800°C . The substrate unit-cell parameters and percent lattice mismatch to the films are shown in Table I. Although most of our previous CMR studies were on the 33% Ca-doped material, the Sr doped analog, with T_C (bulk) close to 380°C (over 100 degrees higher than the T_C of the Ca-doped material which is around 270°C), is the best candidate for room temperature devices and ideal for ambient magnetic imaging characterization [12]. For both cases of substitution the doping level was selected to optimize the transition temperatures [10,11], but previous experience has shown that, compared to their single crystal counterparts, even the best films have slightly suppressed transition temperatures and somewhat flattened $M(T)$ and broadened $\rho(T)$ curves. Under less than ideal conditions, T_C can be anywhere from tens of degrees to over 100 degrees below ideal [12].

Table I. Comparison of the film lattice parameter in the growth direction to the normal lattice parameter of potential perovskite substrates

CMR Film	Plane	Dimensions (nm)	----
$\text{La}_{0.67}\text{Sr}_{0.33}\text{MnO}_3$	{100}	0.3876 [13]	----
$\text{La}_{0.67}\text{Ca}_{0.33}\text{MnO}_3$	{100}	0.3867 [14]	----
Substrate	Plane	Dimensions (nm)	% Mismatch
LaAlO_3	{100}	0.3792	-1.8
SrTiO_3	{100}	0.3905	+1.2

From previous T_S -dependent growth studies of LCMO [4,5,12], we found the as-grown films, at least for $T_S < 850^\circ\text{C}$, to consist of either small grains or epitaxial islands tens of nanometers in size with root-mean-square (RMS) roughnesses less than 20 Å. The microstructure of the films followed the expected T-dependent trend, i.e. increasing grain size and epitaxy with increasing

temperature. For some of the Ca-doped films, the islands were clearly epitaxial by $T_s = 600^\circ\text{C}$ as revealed by the STM; they were faceted, layered, and aligned along substrate crystallographic directions. Island sizes, in general, were usually smaller than the film thickness. The small grain size was, in part, a function of the growth kinetics used in the deposition of these films.

STM and AFM techniques are especially well-suited for characterizing the microstructure of such small grained or islanded, smooth films. MFM [15-17], a variant on the AFM technique, is capable of elucidating intermediate (>20 nm) magnetic features. For that reason it is particularly well suited to play an important role in imaging the micromagnetic structures in these materials and revealing the correspondence between the magnetic structures and their underlying physical bases. It should be able to shed light on details like their orientation, size, and coercivity which is related to the stress directions, sign, and wall pinning. Figure 2 shows a schematic of the AFM/MFM layout including an actual image taken of a CMR film surface and its corresponding magnetic structure. The procedure used in MFM imaging is a two pass process. The tip scans the surface, usually in tapping mode, the line profile of the topography is recorded, then the tip retraces the exact same profile in lift mode at a distance above the surface in the range of 10's to 100's of nanometers within the range of magnetic fields. The result is two images of the same area: microstructure and magnetic structure. MFM imaging, utilizing a magnetically coated AFM tip, is possible because the magnetic field (\vec{H}) of the sample, interacting with the tip stray field produces a force on the tip cantilever which is to lowest order

$$F_z = m_x \frac{\partial H_x}{\partial z} + m_y \frac{\partial H_y}{\partial z} + m_z \frac{\partial H_z}{\partial z} \quad (2)$$

where \vec{m} is the dipole moment of the tip [15]. The variations in the force that the cantilever experiences while it scan over the surface are translated into a map of the micromagnetic structures present in the material. These magnetic domains, whether caused by stress induced through lattice mismatch or local defects such as pin holes or surface boulders, can be studied with the MFM. In many cases they are expected to degrade performance. Such structures result from the presence of magnetic anisotropy (for example the breaking of the crystallographic symmetry due to surface steps), ferromagnetic interactions, magnetoelastic (stress) effects due to lattice distortions, magnetostatic effects, and the influence externally applied fields. In addition, the magnetic field of the MFM tip can be used to influence the magnetic structure of the sample and provide information concerning

the stability of these features. Because the method employed in the MFM imaging process is a two pass method, it is possible to make a one-to-one correspondence between magnetic structure and physical features in the topography. Figure 3 illustrates the ability of the MFM to relate topographic features to their corresponding magnetic structures. In this case the microstructure (Figure 3a) of the annealed LSMO sputter-deposited film is very poor, consisting of non-uniform grains. The magnetic image (Figure 3b) of this film reveals grain size magnetic structures whose coercivity is at least as high as that of our CoCr tip coating. This is illustrated in Figures 3b and c where the tip was first polarized in the "up" direction for imaging (Figure 3b) and then reversed to the "down" direction (Figure 3c) before imaging the same area again. As can be seen by the areas highlighted with boxes, the contrast reverses as the tip polarization does. The polarization of these regions on the sample therefore maintains a constant direction even under the influence of the tip field. In light of the importance of the coupling between transport electrons and magnetic properties, the large change in resistance in the presence of a magnetic field, and the influence of microstructure and stress on the development of local magnetic structures, MFM is an ideal technique for such studies.

EXPERIMENTAL

In the present study, thin films of $\text{La}_{0.67}\text{Sr}_{0.33}\text{MnO}_{3\pm\delta}$ (δ uncertain), were grown on single crystal perovskite substrates with PLD using a 3 inch stoichiometric target. As noted above, this composition was selected to optimize the T_c of the ferromagnetic metallic phase and CMR effect. Films were deposited simultaneously on LAO and STO at 5 Hz repetition rates in 200 mTorr O_2 . Each of the substrates was cut into multiple samples to insure that differences between films were not due to differences in the substrate. In addition, two different substrates were positioned side by side for each growth temperature and more than one film was grown each time to allow several different characterizations to be made. For the growth deposition, T_s values of 500°C, 650°C, or 800°C were used and the thickness of the films determined by Rutherford Back Scattering (RBS) was about 130 nm for the 5 Hz deposition rate. After deposition, the samples were cooled over a 30 minute period to room temperature under 300 Torr of flowing O_2 . (The substrate heater was turned off after the deposition, and allowed to cool by itself). Finally, one half of the samples were annealed at 950°C for 10 hours in 1 atmosphere of flowing O_2 . One run included MgO substrates which were used to characterize the stoichiometry of the films with RBS since this substrate would not influence the Sr or La RBS peaks.

All films were characterized with STM, AFM, MFM, 4-point T-dependent resistivity measurements, and x-ray diffraction. The T-dependent magnetization was measured for the annealed films grown on LAO and STO.

RESULTS and DISCUSSION

X-ray diffraction showed substrate lattice parameters in agreement with published values and a $\sim 0.5^\circ$ miscut of the STO. The deposited LSMO appeared epitaxial in the growth direction at all three temperatures with lattice parameters normal to the surface shown in Table II. Five of the six films grown on STO had lattice parameters smaller than bulk value, and four of the six on LAO had lattice parameters larger than the bulk values. This seems to indicate the expected states of tensile and compressive in-plane strain in the LSMO on the STO and LAO substrates respectively. More x-ray data is being evaluated to determine the in-plane epitaxy and further evidence for strain.

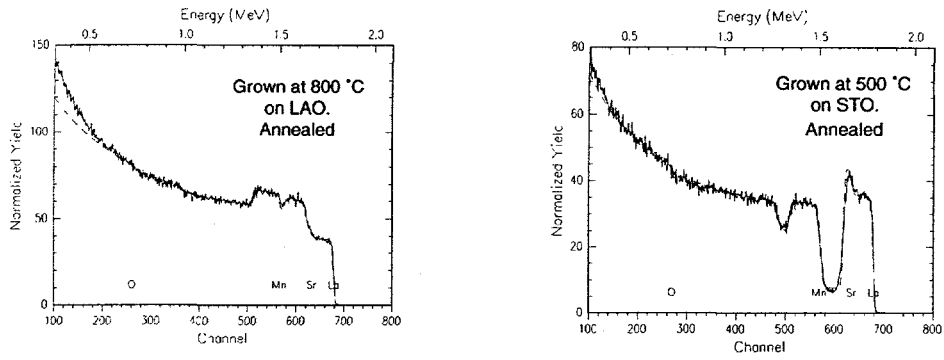
Table II. LSMO x-ray diffraction lattice parameters in the growth direction. Error in last digit is shown in parenthesis. Measured values for STO and LAO are also indicated.

Deposition Temp.	SrTiO ₃ substrate - 3.906 Å		LaAlO ₃ substrate - 3.791 Å	
	As-deposited	Annealed	As-deposited	Annealed
800 °C	3.885(1) Å	3.867(1) Å	3.915(1) Å	3.882(4) Å
650 °C	3.853(1) Å	3.855(1) Å	3.924(1) Å	3.879(1) Å
500 °C	3.871(1) Å	3.862(3) Å	3.868(2) Å	3.868(1) Å

The chemical content of the films was within expectations as the RBS results (Figures 4a and 4b) for one film on LAO and one on STO both showed ratios of La:Sr:Mn:O that were 2/3:1/3:1:3 within experimental error.

In addition, the film grown on MgO (Figure 5) showed that the oxygen anneal parameters did not result in any significant change in oxygen from the as-grown samples.

While the RBS showed correct stoichiometry and it was possible to extract lattice parameters from the x-ray scans, the x-ray peaks were broad, indicating possible structural inhomogeneity in the samples. Some indication of this is also evident in the transport and magnetization measurements shown in Figure 6.



(a)

(b)

Figure 4. RBS data for two annealed LSMO films grown at two different temperatures on (a) LAO and (b)STO.

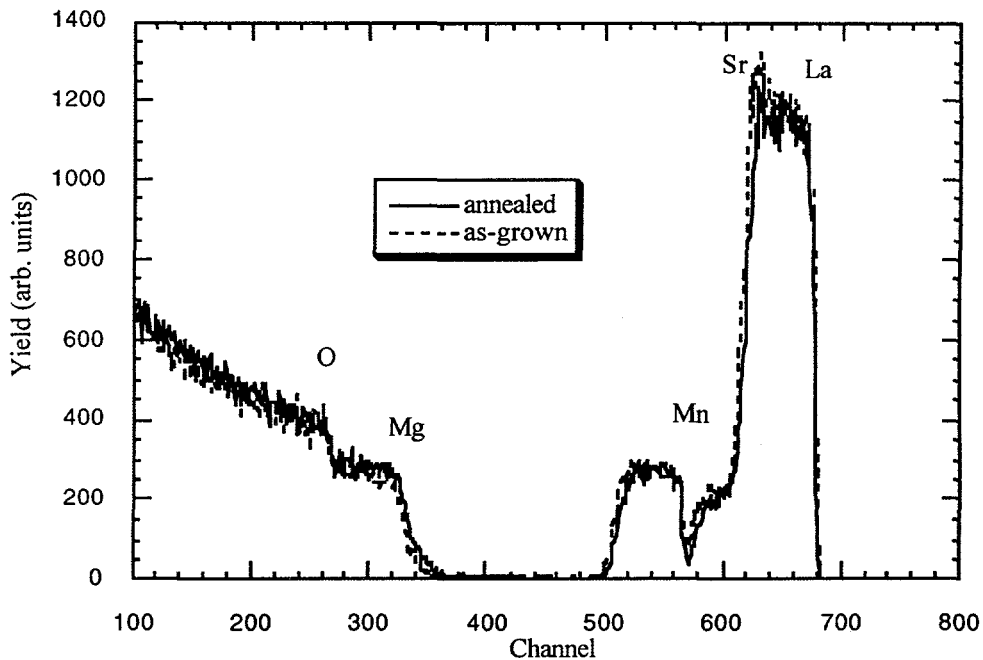


Figure 5. RBS data for as-deposited and annealed LSMO films grown on MgO at 650°C.

All of the films show a metal-insulator transition (panels a and b) coinciding with the drop in magnetization (panels c and d) which is the general behavior of these CMR films. Even anomalies in the resistivity peaks are mirrored in the magnetization when overlaid on a common graph, reflecting the link between the

two. Unfortunately, the transitions on all films occur at lower than expected temperatures (particularly on STO), indicating a T_c below 300 K. This has been attributed to stoichiometry problems in the past and specifically associated with vacancies on the La, Sr, or Mn sites since it is not possible to place an oxygen on an interstitial site [18-20]. However, in our case, based on the RBS results described above and the wide x-ray peaks, it is probably more a matter of crystalline orientation and intergrowths.

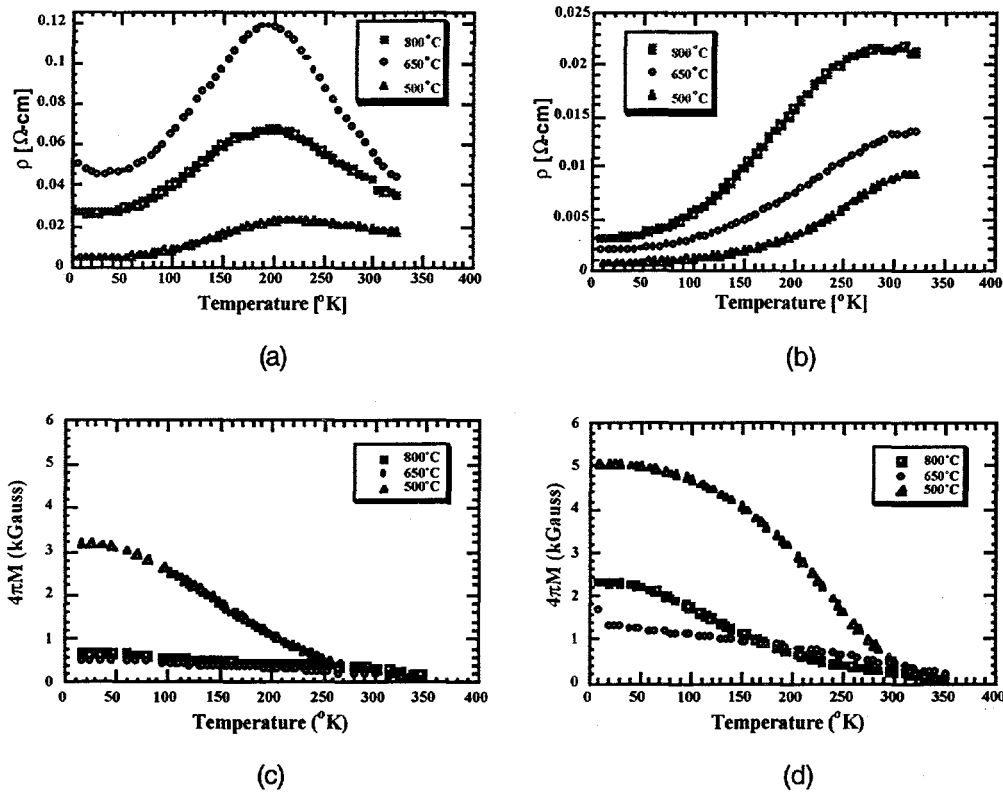


Figure 6. Temperature dependent transport and magnetization data for the annealed LSMO films grown on STO (a and c) and LAO (b and d).

STM and AFM images of the films as-deposited on LAO and STO are shown in Figure 7 and mirror the results of previous studies on Ca doped material. At this stage therefore, there is no indication at the surface of any substrate-induced strain in the as-deposited films. At $T_s = 800^\circ\text{C}$ and 650°C there are very smooth films with RMS roughnesses of 9\AA and 13\AA respectively. The corresponding average grain sizes are 35nm and 20nm . At 500°C on both substrates, however, the grains have begun to cluster, indicating a low mobility. The resulting 3-dimensional growth leads to a roughness of $\sim 75\text{\AA}$. Grain size continues to follow the trend though as close inspection shows that the clustering grains are $\sim 15\text{nm}$

across. On STO we find roughnesses of 9Å, 13Å, and 89Å for the 800 °C, 650 °C and 500 °C depositions respectively with corresponding grain sizes of 44nm, 21nm, and 16nm.

Annealing produces the structures shown in Figure 8. The roughness of the films on LAO are 6Å (800 °C), 11Å (650 °C), and 25Å (500 °C) while on STO, the values are 5Å (800 °C), 4Å (650 °C), and 57Å (500 °C). With the exception of the 650°C deposition on STO, the films all share common features that include faceting and screw dislocations with unit cell Burger's vectors. Again with the exception of the 650°C deposition on STO, the 650 °C and 800 °C films have pinholes near the terrace edges while the 500 °C depositions show much larger voids distributed across the surface. The structure of the films deposited at 500 °C is very similar to low temperature depositions of LCMO on the same substrates. The 650 °C deposition on STO appears very vicinal after annealing and indicates an increased response to the miscut of the substrate. Since the samples were cut from single substrates, it may be that this particular piece came from an edge that was even worse than 0.5° off due to polish variations.

The only AFM evidence for substrate-induced strain is in differences between the 500 °C films after annealing. Panels a) and d) of Figure 8 show (500nm)² scan frames of the annealed 500 °C films on LAO and STO respectively that are representative of the difference which is that on STO, the LSMO shows larger voids and a greater density of voids. This result should be stress-related since both LAO and STO based films had lattice constants very nearly equal to each other and the bulk value.

All of the as-grown and annealed LSMO films were imaged with the MFM, however, no significant magnetic structures were found on our as-grown films on either STO or LAO. This is somewhat surprising since the films' lattice parameters in the growth direction, extracted from x-ray diffraction data, were found to be expanded (LAO) or contracted (STO) as expected for strain in LSMO grown on lattice mis-matched substrates. This finding is in contrast to results obtained elsewhere for films grown on LAO [21] where serpentine arrays of in- and out-of-plane sample-normal magnetic polarization were seen and associated with compressive stresses due to lattice mismatch with the smaller lattice parameter of the LAO substrate (see Table I). For STO (tensile stresses) no comparable magnetic structures were found. A possible explanation for the discrepancy between our results and theirs could be the difference in growth conditions and cool-down rates. These factors point to kinetics and thermal cycling as probable contributions to the observed stress-induced magnetic structures found in that study. In addition, our ferromagnetic ordering and metal-

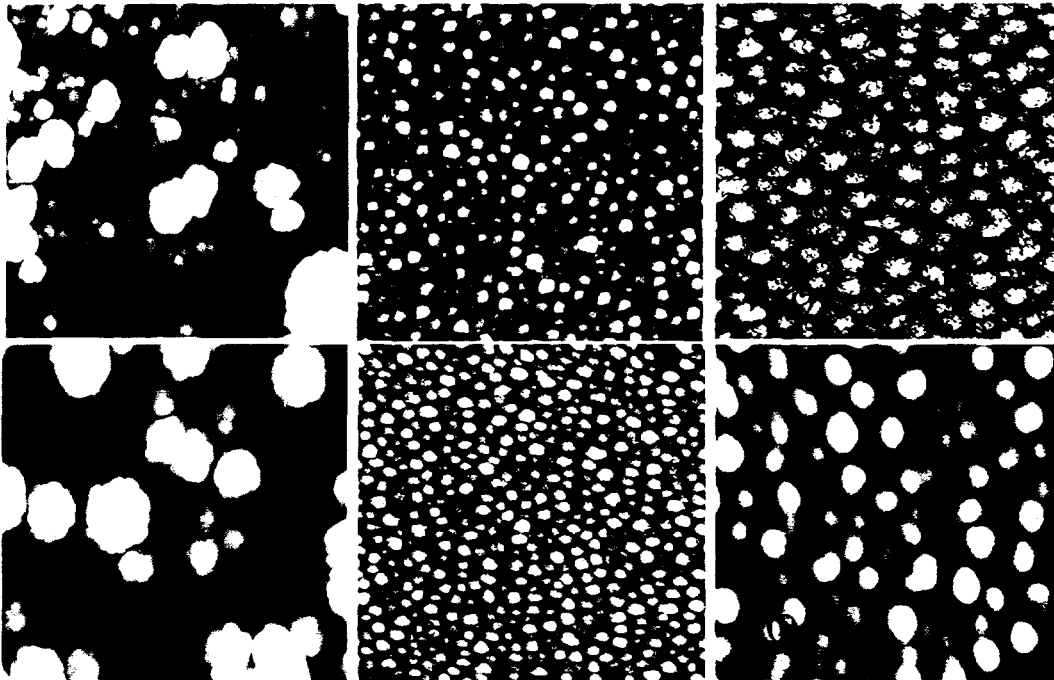


Figure 7. 500 nm x 500 nm images of the surface of LSMO films grown on LAO (a) - (c) and STO (d) - (f): T_s = (a) and (d) - 500°C, (b) and (e) - 650°C, (c) and (f) - 800°C.

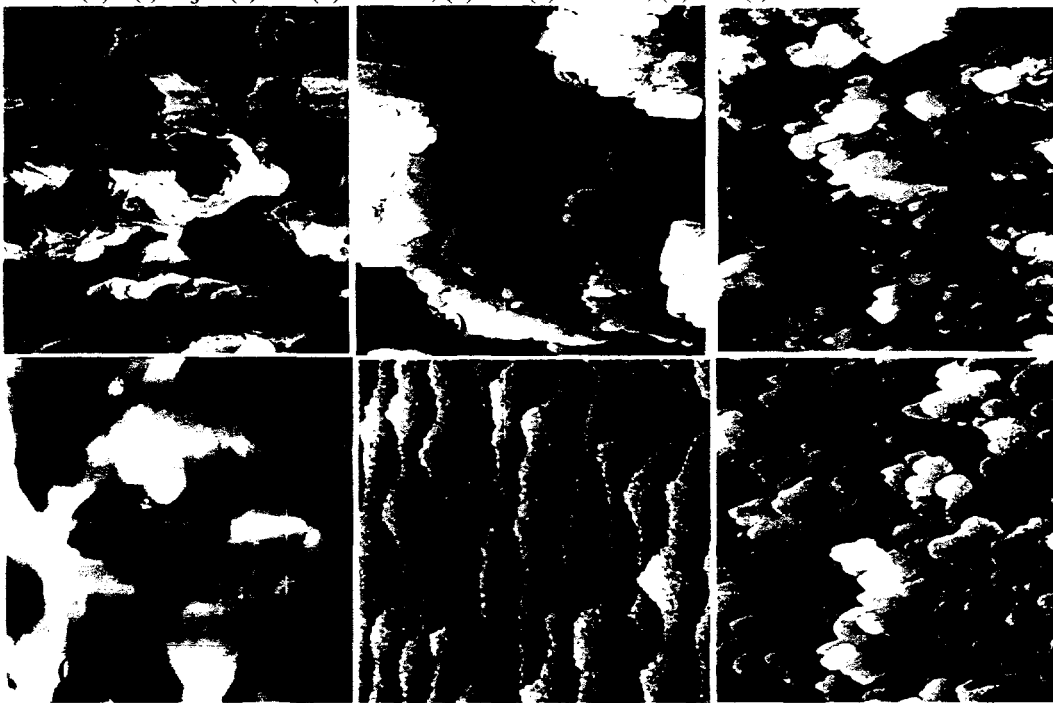


Figure 8. 500 nm x 500 nm images of the surface of LSMO films shown in Figure 7 after annealing in flowing O_2 at 950°C for 10 hours on LAO (a) - (c) and STO (d) - (f): T_s = (a) and (d) - 500°C, (b) and (e) - 650°C, (c) and (f) - 800°C.

insulator transition temperatures for the as-grown films, particularly for those grown on STO, were lower than expected given the RBS, AFM/STM, and x-ray data results.

Magnetic imaging of the annealed films revealed a number of interesting types of structurally-driven magnetic features. Figures 9, 10, and 11 highlight magnetic features found in these films which could be traced to four different sources. The surface structure of the 500°C annealed film grown on LAO is shown in Figure 9a. The prominent surface pits, averaging 400 nm across, varied from a few nanometers to nearly 300 nm deep. The corresponding magnetic image, shown in Figure 9b, correlates well with the depths of the pits, the deeper the pit the larger and darker the magnetically polarized region. These features were always dark in the magnetic image irrespective of the direction that the MFM tip was polarized. As we don't, at this time, believe these features are artifacts of the imaging process, we interpret this lack of contrast reversal to a reversal of the direction of the polarization of these local features in response to the change in the tip polarization direction. The arrows in the images draw attention to a magnetic feature surrounded by a lighter halo while the area around the pit is actually lower than its surrounding area in contrast to what would be expected if the features were not magnetic in origin. Note that the magnetic features are laterally smaller than their physical counterpart; they are probably due to a breaking of the local symmetry at the step edges of the terraces that form the pit.

The surface of the coalesced layers of the 650°C annealed LSMO film grown on LAO is shown in Figure 10a. As is typical of the annealed films, this film is very smooth with only the unit-high step edges visible in the image. The only prominent features in the magnetic image of this surface (Figure 10b) are the dark circles seen in a featureless background. These dark regions originate from three different sources. A dark arrow points to one of the many small pits scattered across the surface of the film. Although the hole is quite small, the magnetically polarized region is many times larger than the actual feature. That is equally true of the surface debris highlighted by the white arrows. In each case, we believe the magnetic structures are due to magnetoelastic effects caused by local strain in vicinity of these two kinds of structural features, however, not all surface debris results in local magnetic structure.

The two white boxes included two sets of magnetic feature, on the other hand, for which there is no obvious topographical origin. It is unlikely to be caused by the surface steps, which one might have suspect, since there are many more candidate step edges than circle of magnetic polarization. A more likely explanation is that the origin is a buried defect. This illustrates the power of the

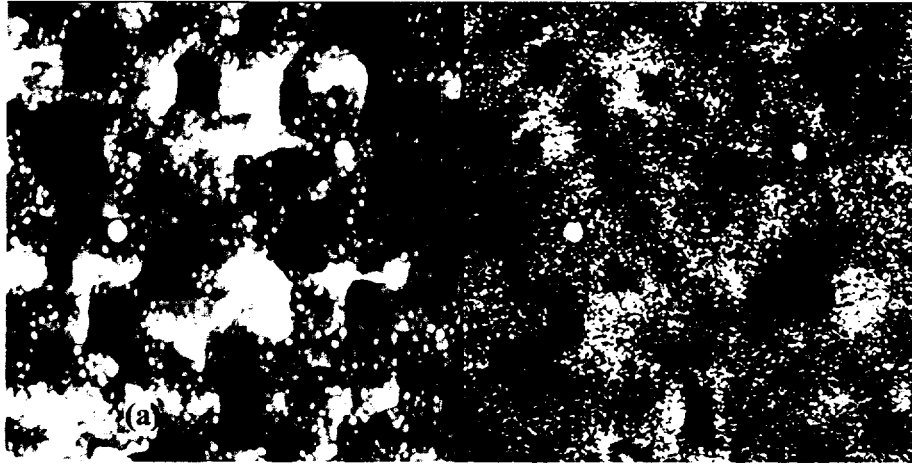


Figure 9. $2\ \mu\text{m} \times 2\ \mu\text{m}$ topography (a) and corresponding magnetic structure (b) images of a post-deposition annealed LSMO film grown at 500°C on LAO. A direct correspondence can be seen between the magnetic features in image (b) and the surface pits in image (a).

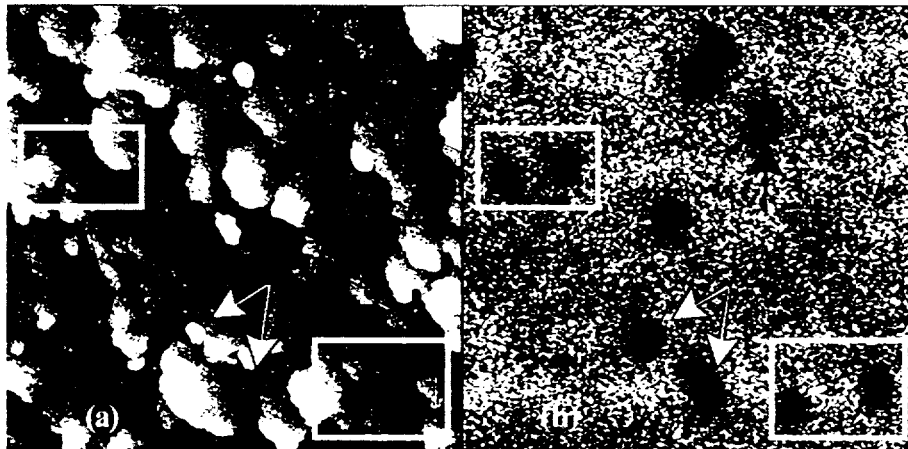


Figure 10. $4\ \mu\text{m} \times 4\ \mu\text{m}$ topography (a) and corresponding magnetic structure (b) of a post-annealed LSMO film grown at 650°C on LAO. Magnetic features correspond to positions of a small pinhole (black arrow), surface particles (white arrows), and what appears to be surface steps (white boxes). However, the latter are probably due to buried defects.

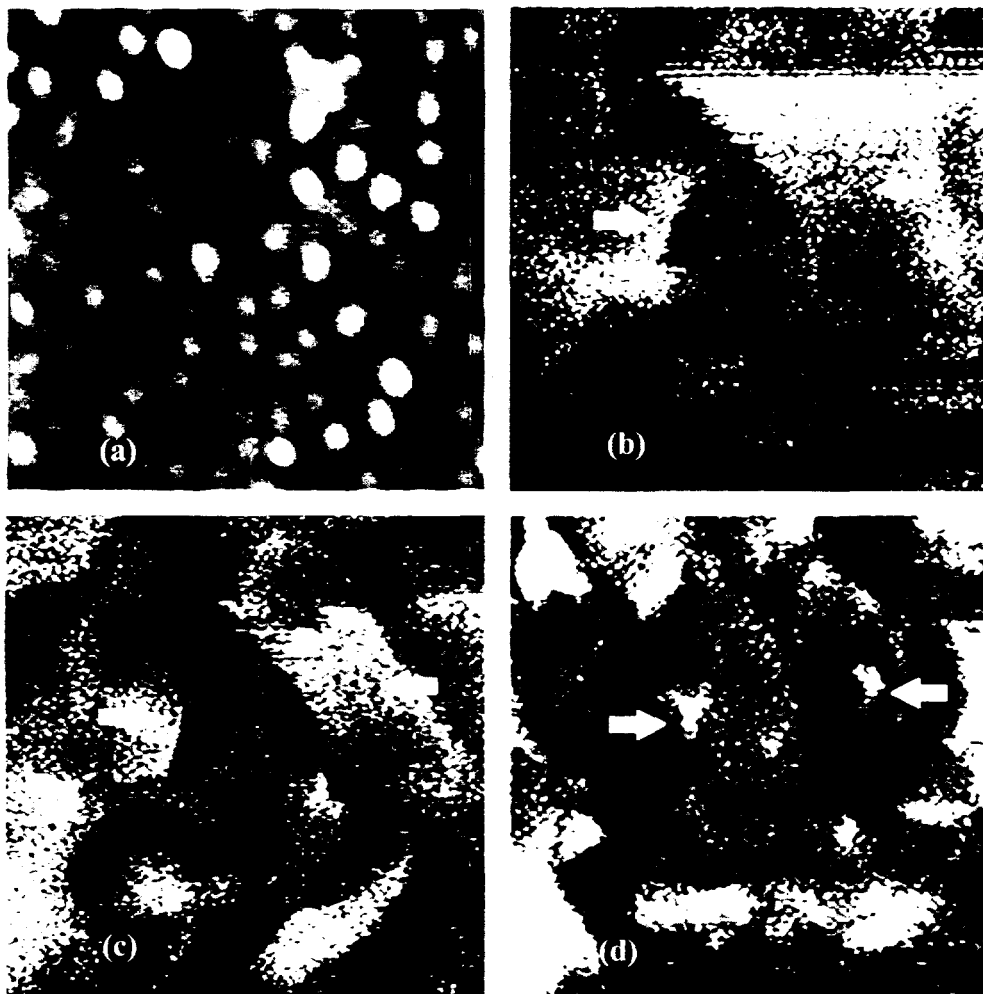


Figure 11. 550 nm x 550 nm surface topography (a) and corresponding magnetic structure (b) - (d) of a post-annealed LSMO film grown at 800°C on a LAO. (b) was taken with the tip 75 nm, (c) 50 nm, and (d) 25 nm above the surface, respectively. The arrows indicate some of regions where the local magnetization direction rotates from repulsive (light) to attractive (dark) under the influence of the increasing tip field as it nears the surface.

MFM to image below the surface to reveal subsurface magnetic structures. These magnetic structures were also insensitive to the tip polarization direction.

As has been noted above, the MFM is capable of influencing the position/size of magnetic domains if the coercivity of the sample features is less than that of the tip. This can be a powerful capability to study the stability of magnetic domains in the presence of an external field. By changing the lift height for the magnetic imaging, the field experienced by the sample can be varied. This is shown in Figures 11b, c, and d. The surface of this 550 nm x 550 nm area of the 800°C grown annealed LSMO on LAO film is shown in Figure 11a. Except for the surface bumps (probably a tip artifact) the region is atomically smooth. The arrows in Figures 11b, c, and d are positioned at locations on the surface that change from light (repulsive) to dark (attractive) as the tip is moved closer to the surface, starting at 75 nm then lower to 25 nm. The highlighted features shrink in size as the spins gradually rotate to an attractive interaction with the tip. This process was completely reversible. The streaking visible in Figures 11a and b was also reproducible and is probably due to the polarization changing as the tip passes over the surface. Although a high coercivity tip was used for this imaging, in general one can't tell definitively which polarization direction is changing, tip or sample, without using tips with different effective moments.

CONCLUSIONS

Pulsed laser deposition was used to produce LSMO over a wide range of temperatures. The films were epitaxial in the growth direction and had grains that increased in size with increasing deposition temperature. Upon annealing, the grains coalesce into terraces with pinholes and screw dislocations upon annealing. These features are consistent with previous studies of LCMO films. Most higher-temperature depositions showed the expected substrate-dependent strain in X-ray-derived lattice constants but the low temperature depositions appeared to have relieved their stress through formation of large voids. No correlations between film morphology and transport or magnetization were evident, indicating that these particular films may have been strongly influenced by strain and/or defects at the growth interface. These effects were not obvious at the surface though.

Magnetic features associated with pinhole and void defects on the films was observed with MFM. The magnetic signatures associated with the observed pinholes also imply the existence of subsurface voids of similar size and the ability to detect them with MFM. The general magnetic domain structure of the films was not obvious in MFM. This is likely the result of imaging above the

films' critical temperatures, which came out lower than expected. Since the film stoichiometry and epitaxy was acceptable, these low critical temperatures may also be related to strain at the growth interface. Transmission electron microscopy experiments would be one way to address this issue in future studies.

REFERENCES

¹M.F. Hundley, M. Hawley, R.H. Heffner, Q.X. Jia, J.J. Neumeier, J. Tesmer, J.D. Thompson, and X.D. Wu, "Transport-Magnetism Correlations in the Ferromagnetic Oxide $\text{La}_{0.7}\text{Ca}_{0.3}\text{MnO}_3$," *Applied Physics Letters*, **67** [6] 860 (1995).

²M.F. Hundley, J.J. Neumeier, R.H. Heffner, Q.X. Jia, X.D. Wu, and J.D. Thompson, "Interplay Between Electronic Transport and Magnetic Order in Ferromagnetic Manganite Thin Films," to be published in *Epitaxial Oxide Thin Films III*, Edited by C.-B. Eom, C. Foster, M.E. Hawley, D.G. Schlom, and J.S. Speck, Materials Research Society Symposium Proceedings (1997).

³M.E. Hawley, "Scanning Tunneling and Atomic Force Microscope Studies of Thin Sputtered Films of $\text{YBa}_2\text{Cu}_3\text{O}_7$," pp. 28-70 in *Interfaces in High Temperature Superconductors*, Edited by S.L. Shinde and D.A. Rudman, Springer-Verlag New York, Inc., New York, 1994.

⁴M.E. Hawley, X.D. Wu, P.N. Arendt, C.D. Adams, M.F. Hundley, and R.H. Heffner, "Microstructural Study of CMR Films as a Function of Growth Temperature, As-Deposited and Annealed," pp. 531-536 in *Epitaxial Oxide Thin Films II*, Edited by J.S. Speck, D.K. Fork, R.M. Wolf, and T. Shiosaki, Materials Research Society Symposium Proceedings, **401** Materials Research Society, Pittsburgh, 1996.

⁵M.E. Hawley, C.D. Adams, P.N. Arendt, E.L. Brosha, F.H. Garzon, R.J. Houlton, M.F. Hundley, Q.X. Jia, J. Neumeier, and X.D. Wu, "CMR Films' Structure as a Function of Growth and Processing," to appear in *Journal of Crystal Growth*, Springer-Verlag 1997.

⁶S. Jin, T.H. Tiefel, M. McCormack, R.A. Fastnacht, R. Ramesh, and L.H. Chen, "Thousandfold Change in Resistivity in Magnetoresistive La-Ca-Mn-O Films" *Science*, **264** 413-15 (1994).

⁷H.L. Ju, C. Kwon, Q. Li, R.L. Greene, and T. Venkatesan, "Giant magnetoresistance in $\text{La}_{1-x}\text{Sr}_x\text{MnO}_z$ Films Near Room Temperature," *Applied Physics Letters*, **B65** [16] 2108-10 (1994).

⁸Y.-F. Chen, L. Sun, Y. Pan, Y. Tao, Z.-G. Liu, and N.-B. Ming, "Preparation and Characterization of Epitaxial $\text{La}_{0.65}\text{Sr}_{0.35}\text{MnO}_z$ Thin Films Grown by Pulse Laser Deposition," *Materials Letters*, **27** 139-43 (1996).

⁹A.J. Millis, P.B. Littlewood, and B.I. Shraiman, "Double Exchange Alone Does Not Explain the Resistivity of $\text{La}_{1-x}\text{Sr}_x\text{MnO}_3$," *Physical Review Letters*, **75** [25] 5144-7 (1995).

¹⁰P. Schiffer, A.P. Ramirez, W. Bao, and S.W. Cheong, "Low-Temperature Magnetoresistance and the Magnetic Phase-Diagram of $\text{La}_{1-x}\text{Ca}_x\text{MnO}_3$," *Physical Review Letters*, **75** [18] 3336-9 (1995).

¹¹A. Urushibara, Y. Moritomo, T. Arima, A. Asamitsu, G. Kido, and Y. Tokura, "Insulator-Metal Transition and Giant Magnetoresistance in $\text{La}_{1-x}\text{Sr}_x\text{MnO}_3$," *Physical Review B*, **51** [20] 14103-9 (1995).

¹²G.W. Brown, Q.X. Jia, E.J. Peterson, D.K. Hristova, M.F. Hundley, J.D. Thompson, C.J. Maggiore, J. Tesmer, and M.E. Hawley, "Growth and Magnetic Structure of $\text{La}_{0.67}\text{Sr}_{0.63}\text{MnO}_3$ Films," Edited by C.-B. Eom, C. Foster, M.E. Hawley, D.G. Schlom, and J.S. Speck, to be published in *Epitaxial Oxide Thin Films III*, Edited by J.S. Speck, D.K. Fork, R.M. Wolf, and T. Shiosaki, Materials Research Society Symposium Proceedings (1997).

¹³M.C. Martin, G. Shirane, Y. Endoh, K. Hirota, Y. Moritomo, and Y. Tokura, "Magnetism and Structural Distortion in the $\text{La}_{0.7}\text{Sr}_{0.3}\text{MnO}_3$," *Physical Review B*, **53** [21] 14285-90 (1996).

¹⁴L.H. Chen, S. Jin, T.H. Tiefel, R. Ramesh, and D. Schurig, "Large Magnetoresistance in La-Ca-Mn-O Films," *IEEE Transactions on Magnetics*, **31** [6] 3912-14.

¹⁵K. Babcock, M. Dugas, S. Manalis, and V. Eilings, "Magnetic Force Microscopy: Recent Advances and Applications," pp. 311-22 in *Recent Advances and Application*, Proceedings of the Materials Research Society, **355** 311-22 (1995).

¹⁶E. Dahlberg and J.-G. Zhu, "Micromagnetic Microscopy and Modeling," *Physics Today*, **April 1995** 34-40 (1995).

¹⁷P. Grutter, "An Introduction to Magnetic Force Microscopy," *MSA Bulletin*, **24** 416-25 (1994).

¹⁸J.A.M. Van Roosmalen and E.H.P. Cordfunke, *Journal of Solid State Chemistry* **110** (1994) 106.

¹⁹J.A.M. Van Roosmalen and E.H.P. Cordfunke, *Journal of Solid State Chemistry* **110** (1994) 109.

²⁰J.A.M. Van Roosmalen and E.H.P. Cordfunke, *Journal of Solid State Chemistry* **110** (1994) 113.

²¹C. Kwon, K.-C. Kin, M.C. Robson, J.Y. Gu, S.E. Lofland, S.M. Bhagat, Z. Trajanovic, M. Rajeswari, T. Venkatesan, R. Ramesh, A.R. Kratz, and R.D.